Role of Magnetic Resonance Imaging and *in vivo* MR Spectroscopy in Clinical, Experimental and Biological Research

N R JAGANNATHAN*

Department of NMR, All India Institute of Medical Sciences, New Delhi 110 029

Magnetic resonance imaging, a noninvasive imaging modality in clinical medicine produces soft tissue anatomical pictures in any desired plane that are exquisite representation of the spatial distribution of mobile protons present in human/animal tissues. *In vivo* magnetic resonance spectroscopy, on the other hand, is a useful technique for studying metabolic processes in biological systems. In the last decade, magnetic resonance imaging and *in vivo* spectroscopy methods have become an established tool in many areas of biomedical research for example, in understanding the physiology of several disease processes, tumor metabolism, and drug discovery process. In fact, *in vivo* magnetic resonance spectroscopy can be used for diagnosis of a specific disease pattern with biochemical/metabolic signature (marker), assessment of tumor response to different treatment regimens, drug concentrations in tissues, drug efficacy and metabolism. The advantage of *in vivo* magnetic resonance is its versatility and comprehensive characterization of normal and diseased tissues. In this article, a few examples of *in vivo* magnetic resonance methods and their utility in clinical, experimental and biological research are presented.

Key Words: Magnetic resonance imaging, *In vivo* MR spectroscopy, Morphology, Applications, Clinical, Experimental, Biological, Metabolism, Tumor, Cancer, Functional MRI

Introduction

Nuclear magnetic resonance (NMR), since its discovery in 1940s, has played an important role in many areas of physics, chemistry, and material science. Initially NMR was used for chemical structure elucidation, but simultaneously, its potential in biological research, especially medicine, was recognized. Shown and Elsken in 1950 investigated the water content of potato and maple wood. Singer (1959) measured blood flow in the tails of mice. In 1973, high-resolution phosphorus (^{31}P) NMR studies of intact blood cells were reported (Moon & Richards 1973). Later, Hoult et al. (1974) reported ^{31}P NMR of freshly excised rat leg muscle. Burt et al. (1976) reported similar observations for other muscle types. Ackerman et al. (1980) reported noninvasive ^{31}P NMR study of skeletal muscle and brain metabolism in small animals using a surface coil. With the availability of larger magnets extension to human ^{31}P MR studies, followed later.

MR imaging developments are largely based on the work of Damadian who reported that the NMR relaxation time constants (T1 and T2) are different for normal and malignant tissues and could have diagnostic value (Damadian 1971). In 1973, Lauterbur produced the first NMR image of an object and called it as 'zeumatography', using magnetic field gradients (Lauterbur 1973). Later, MR images of human organs such as the finger (Mansfield & Maudsley 1976), hand (Andrew et al. 1977) and wrist (Hinshaw et al. 1977) were reported. By mid 1980's, added by developments in magnet technology, RF electronics and powerful computers, the full potential of magnetic resonance imaging (MRI) as a clinical tool was realized. Today, MR is experiencing a rapid expansion and has achieved an amazing level of success as an important tool to study disease processes in clinical and experimental research. This rapid growth is due to its noninvasive nature, use of no ionizing radiation and its ability to generate

E-mail: jagan1954@hotmail.com;   *Tel:* (011) 2659 3253/26850533; *Fax:* (011) 2686 2663

high-resolution images. Also, the technique of *in vivo* NMR spectroscopy (MRS) can be used as a unique means to probe the biochemistry of living systems and to gain diagnostic information (Danielsen & Ross 1999). This diagnostic information is derived from MRI and MRS or a combination of both the approaches. MRI produces a spatial display of the distribution of nuclei and provides a morphological picture (anatomical information) similar to those of CT scanning but with superior contrast resolution. In addition, recent advances in MRI methodology offer higher spatial resolution (100 μm or less), enabling detailed morphological/ anatomical information from small animals.

In vivo MRS of cells, organs and tissues both, in humans and animals, is an extension of high-resolution NMR used for molecular structure determination, but applied to more complex systems. For example, it can be used to observe different metabolites present in a particular region of tissues and organs. The determination of the concentration and relative levels of these metabolites provides information about normal and abnormal tissues. This technique can also be used to monitor the response of tumors to various therapeutic modalities and to understand the different metabolic processes (Stark & Bradley 1998, Jagannathan 2001). For these reasons, both MRI and MRS are increasingly being used in clinical, experimental, pharmaceutical and biological research. It is this link between clinical and pre-clinical applications that renders MR as an attractive tool (Jagannathan 2001). Even though MRI and MRS have evolved more or less independently, *in vivo* localized MRS in humans and other living systems are mainly guided through MR images. Thus, the success of MRI has led to considerable interest in MRS as a noninvasive probe to monitor the metabolism of living systems. In short, MRI produces the spatial map of the proton (hydrogen-^{1}H) distribution present in tissues/organs using magnetic field gradients that are strong compared to the molecular interactions, while MRS deals with molecular interactions in the absence of magnetic field gradients.

This review covers the basic concepts of MRI and *in vivo* MRS in qualitative terms without the use of quantum physics. In fact, it is beyond the

scope of this article to present a comprehensive review of the theory and the various applications of MRI and MRS. The organization and content of the review are arranged in such a fashion that would enable both, the readers, who are novice to MR, and the active researcher who wishes to refer to the article as a reference material.

Theory

NMR can be defined as the magnetic interaction between the nuclei of atoms and the radio frequency (RF) field in the presence of an external magnetic field (B_0). The theory is based on the spin (I) properties of nuclei. Spin is defined as an intrinsic angular momentum of a nucleus that is responsible for the magnetic moment. Nuclei of some elements, for example, proton (^{1}H) and phosphorus (^{31}P) behave as magnetic dipoles and without any external influence are randomly oriented in tissues. However, in presence of strong magnetic field ($\mathbf{B_o}$) such as the powerful magnet of the MRI scanner, these magnetic dipoles lines up either parallel or anti-parallel to the externally applied magnetic field (figure 1). More spins lines up in parallel orientation, due to its lower energy state. By applying a radio frequency RF pulse, these nuclei
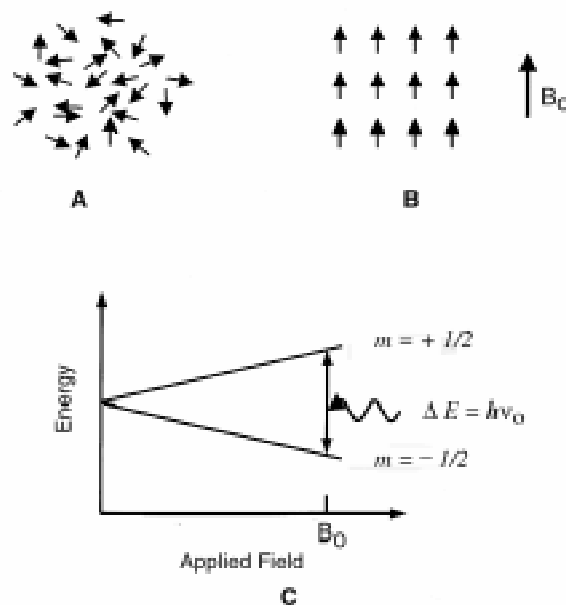

Figure 1 A-C. A, Orientation of individual spins in human tissue sample in the absence of external magnetic field; **B$_o$** In the presence of an external magnetic field (**B$_o$**), the spins orient themselves along the magnetic field direction with some parallel and some anti-parallel to the magnetic field. Transition between the energy levels is possible by the application of RF energy (equivalent to ΔE) applied at the resonant frequency (v_0) of the proton nucleus.

can be flipped from a parallel to an anti-parallel state. After the pulse, the nuclei return to the parallel state thereby emitting RF energy. The frequency of the energy depends upon the strength of the magnetic field of the main magnet of the scanner. By manipulating the magnetic field strength across the body, different tissues of the body can be labeled with different radio frequencies. The sum of these frequencies is detected, sent back to the computer and analyzed to produce images. For in-depth details of the physical principles of MR, the reader may refer to standard text-books referred above as well as other review articles (Raghunathan & Jagannathan 1996, Raghunathan 1998).

Since the human body contains approximately 70% water, most MR images are acquired using proton nuclei present in the water molecule. Each water molecule have two associated hydrogen atoms covalently bonded to an oxygen atom, and there are approximately 5×10^{27} hydrogen nuclei in an adult human body. Most clinical MR images rely on the strong signal of mobile protons in the body that arise primarily from water and fat. The images are pictorial representation of the spatial distribution of these mobile protons. The density of mobile protons in the tissue affects the image contrast, in addition to other factors discussed later in this article.

Relaxation Times

Most MR images are either T1- or T2- weighted (vide infra). T1 and T2 refer to magnetic resonance time constants that are intrinsic to a particular tissue. T1 is the spin-lattice (longitudinal) relaxation time. As nuclei returns to the lower energy state, energy is lost by the nuclei due to its interaction with the surrounding environment or lattice. This process is called as spin-lattice or T1 relaxation time. T2 denotes the spin-spin (transverse) relaxation time. This refers to the loss of energy due to interaction with other nuclei aligned with the magnetic field. T2 relaxation is actually confounded by $T2^{*}$ relaxation, which is much shorter and results from inhomogeneity in the main magnetic field.

While T1 and T2 relaxation times have been separated for purposes of discussion, it is important to realize that they are occur simultaneously during any given imaging procedure, and both contribute to the imaging process. T1 and T2 are specific tissue characteristics. Their value will vary depending on factors such as magnetic field strength. Nevertheless, at a given field strength, different tissues have different characteristic T1 and T2 (see table 1; values from Stark & Bradley 1998) values.

Magnetic Field Strength and Gradients

MRI systems are generally characterized by the strength of the magnetic field. Most imaging procedures are performed at field strengths in the range of 0.2 to 1.5 Tesla, although imaging outside this range is possible. The strength of the magnetic field determines the resonance frequency of water proton in the tissue.

Prior to the actual image acquisition process, the magnetic field is homogeneous at all points inside the magnet bore, for example, throughout a patient's body. However, during the data acquisition the gradient coils are switched on and off in a pulsed fashion. The gradient coils are located within the bore of the magnet, and when a current is passed through the coils, the main magnetic field ($\mathbf{B_o}$) changes linearly along the gradient. The purpose of these gradient magnetic fields is two fold- slice selection and pixel localization within the slice. A combination of magnetic field gradient and RF excitation at specific frequency permits slice selection. The presence of a gradient field during relaxation helps to localize the protons within the slice that were selected during excitation.

Furthermore, steeper the gradient field, thinner will be the slice. Similarly, narrow bandwidth RF pulses, produce thinner slices. The gradient coils consist of three pairs of each of the following: X, Y and Z gradient. Mostly, Z gradient changes the gradient magnetic field along the main magnetic field (Z-axis) thereby allowing a slice selection for imaging. X-gradient coils produce a magnetic field

Table 1 *Relaxation times T1 and T2 at field strength of 1.5 Tesla for various tissues together with proton density (PD)*

Tissue	PD (%)	T1 (ms)	T2 (ms)
Brain gray matter	69	760	77
Brain white matter	61	510	67
Fat	90	260	80
Skeletal muscle	100	860	50
CSF	100	2650	280
Edema	86	900	77

gradient across the patient (horizontal axis), providing spatial localization along the X-axis of the patient. This technique is usually called 'frequency encoding'. The Y-gradient coils produce antero-posterior magnetic field gradient along patients, and by convention, the Y-axis is used for 'phase encoding' the NMR signal. Together, the Y- and X-gradients precisely determine, where within the imaging plane the NMR signal from each voxel or pixel originates. The Z-gradient is always used for selection of a transaxial plane and is called as 'slice selection gradient'. To select either of the axial, sagittal or coronal planes for imaging, the Z-, X-, or Y-gradients, respectively, will be energized as magnetic fields add vectorially. When all the three gradients are energized at the same time, an oblique plane is defined.

Pulse Sequences

A pulse sequence is a set of instructions that accomplishes two tasks. First, the sequence collects the data in an orderly fashion to determine the origin of the signal, i.e., the pixel position, which is a function of the gradient magnetic fields outlined earlier. Secondly, the sequence influences the image contrast or pixel character by specifying the timing and power of the RF pulses. Many of the parameters that need to be specified in a pulse sequence, such as the timing and magnitude of gradient magnetic fields (normally denoted as G_x or G_y or G_z) are included in the computer software.

A number of MRI pulse sequences are in use and can be categorized into two main groups: (i) the spin-echo (SE) and (ii) the gradient recalled echo (GRE). The images are acquired using either a single-echo or a multi-echo approach (Stark & Bradley 1998, Edelman et al. 1995). The most commonly used sequences are spin echo, partial saturation, inversion recovery, FLASH (fast low angle shot), and GRASS (gradient recalled acquisition in the steady state). The SE pulse sequence shown in figure 2 is often used in clinical diagnosis. The various timings and pulse shapes of gradients are shown in figure 2. In order to get quality image with good contrast, one needs to specify (a) type of pulse sequence, (b) time intervals such as TR, TE, (c) matrix size, (d) number of signal averages, (e) plane of image, (f) spatial separation of the slice, etc. Multi-slice and multi-echo technique help to decrease total
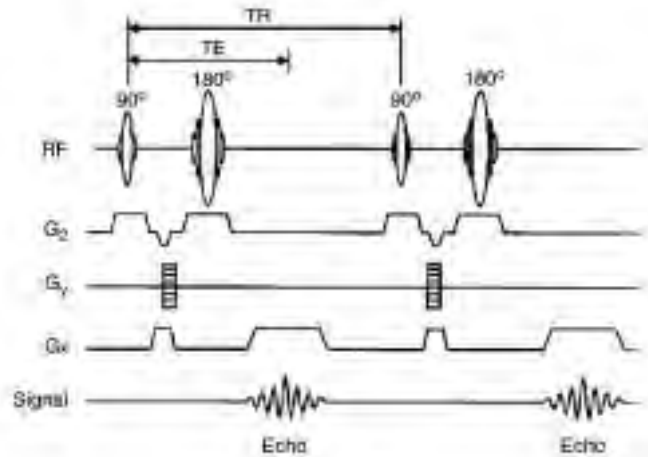

Figure 2 Multi slice SE RF pulse sequence showing the various time delays such as time of echo (TE), time of repetition (TR), etc. G_x, G_y, and G_z refers to the gradient field applied along X, Y and Z-axes. "Echo" refers to the NMR signal (FID).

scan time. Echo-planar imaging (EPI) (Mansfield 1977) which is widely used for image data acquisition in very short time-scale, typically less than 100 ms, is one of the approaches for rapid scanning. EPI acquires a complete set of GREs with a single shot or in a series of multiple shots. EPI sequences are used in functional MRI, bolus tracking, diffusion and perfusion studies (von Schulthess 1997, Edelman et al. 1994).

Contrasts in MRI

The primary sources of inherent tissue contrast in MRI are three-fold: proton density (PD), T1- and T2-relaxation. While PD within soft tissue vary by only a few percent, the proton contribution to the measured MR signal tends to vary by a greater amount, from a few percent up to 30% among soft tissues. Furthermore, T1 and T2 relaxation times often vary even more widely, sometimes by more than 100% among soft tissues (table 1), and it can have important effect on image contrast (figure 3). For example, the T1 of cerebrospinal fluid (CSF) is many-fold higher than white matter. Similarly, inflated tissue (edema) has higher T1 and T2 than normal white matter. Few types of lesions, such as lipomas, melanomas, and fibrous lesions deviate from this general rule of having higher T1 and T2 values than the surrounding normal tissues. Although data on proton density are limited, it often occurs that PD values are directly correlated with relaxation times. For example, normal tissues or lesions having longer T1 and T2 values also tend to have
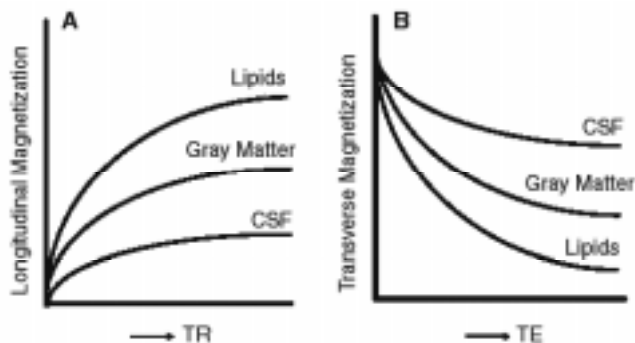
Figure 3 Relative MR signal intensities of tissues: (**A**) as a function of the repetition time (TR) and (**B**) as a function of the echo time (TE).

higher PD values as has been demonstrated for brain white matter lesions (Geis et al. 1989) and appear to be generally true for most other lesions.

The pixel intensity in a MR image is a function of T1, T2 and image acquisition parameters such as TR and TE. The effect of TE and TR on image contrast in a typical SE imaging pulse sequence is given in table 2. In routine MRI, the images obtained are either PD, T1-weighted or T2-weighted images. They usually do not refer to images that display pure PD, T1 or T2. Instead, the terms refer to the relative weightage with which these three parameters affect the tissue contrast in MR images. Such images are obtained by varying the TE and TR as given in table 2B. Generally, tissues with short T1 will appear bright on T1-weighted image, and tissues with long T1 will appear dark. For example, in a T1-weighted image (from our work on a volunteer) of a brain, the fat will appear as white, white matter as light gray, gray matter as dark gray, and CSF as black as shown in figure 4A. In a T2-weighted image of a brain (figure 4B), fat appears as gray, white matter as dark gray, gray matter appears as gray, and CSF as white. In general, T1-weighted images are useful for viewing anatomy (morphology) while T2-weighted images are useful for identifying the tissue pathology. MR images are produced by assigning shades of gray, white, and black to the strength of the signal produced by the relaxing protons.

Applications of MRI

The advantage of MRI compared to the other imaging modalities is the ability to image in any orthogonal plane – axial, coronal, or sagittal as well as in any desired oblique plane. Owing to excellent soft tissue contrast, even small structures, such as cranial

Table 2 A. *Effect of TR and TE on image contrast in spin-echo imaging*

Primary source	TE settings	TR settings
T1	Short TE (< 25 ms)	Comparable to T1s of the two tissues (towards shorter T1 is better)
T2	Comparable to T2s of the two tissues (towards the longer T2 is better)	Long compared to the T1s of the two tissues (2000 ms or greater)
Proton Density (PD)	Short TE (< 25 ms)	Long compared to the T1s of the two tissues (2000 ms or greater)

Table 2 B. *A general rule to get PD, T1 and T2 weighted MR images.*

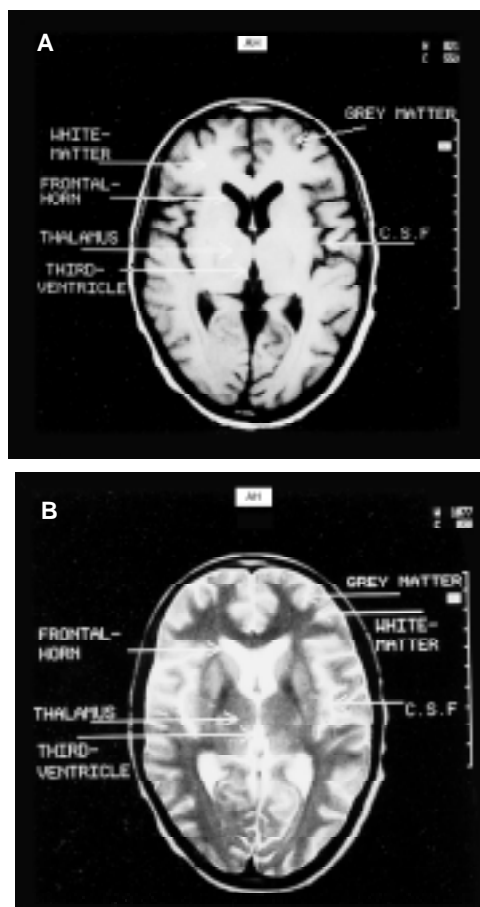|		
Long TE (> 70 ms)		T2 Weighting
Short TE (< 25 ms)	T1 Weighting	PD Weighting
	Short TR (300-700 ms)	Long TR (2-3.5 s)

Figure 4 Transverse (axial) SE MR images of a volunteer: (A) T1 – weighted [slice thickness = 5 mm; TR = 550 ms; TE = 15 ms; field of view (FOV) = 250 mm] and (B) T2– weighted (slice thickness = 5 mm; TR = 2600 ms; TE = 90 ms; FOV = 250 mm).

nerves, are clearly seen. It is extremely useful technique for diagnosing abnormalities in the central nervous system (CNS) and spinal cord (Stark & Bradley 1998, Edelman et al. 1995). The T1- and T2-relaxation times are long in most tumors and lesions compared to the normal tissues. Thus tumors, demyelinating diseases and other pathologies show good contrast on T2-weighted images. It is a superb method to study brain tumors because of excellent soft tissue contrast resolution. Because of the absence of artifacts due to bones, MRI is the method of choice, for imaging vertex, posterior fossa, walls of the middle fossa at the base of the skull, and orbits. Smaller tumors are demonstrated better in MRI than C T , usually without the need of contrast material. MRI is also a good method for evaluating acoustic neuromas, pituitary tumors, non-neoplastic disease, ischemia, hemorrhage, arteriovenous mal-formations , trauma, dis-orders of myelination, dementia, infection, etc. The applications of MRI for the study of spine are numerous, and the normal anatomy of the spine (figure 5) is best defined in sagittal plane (Monelfe 1992).

Cardiovascular MRI has emerged as a new subspeciality, which provides anatomical and functional assessment of the heart, evaluation of myocardial viability, and coronary artery disease (Duerinckx 1999, Van der Wall & de Ross 1991). Cardiac MRI also offers direct visualization and characterization of atherosclerotic plaques, diseased vessel walls, and surrounding tissues (Fayad & Fuster 2000). MRI can characterize plaque and identify the presence of a thrombus or calcification. Most cardiac imaging is obtained using electro-cardiogram (ECG) or pulse triggering to avoid image artifacts due to heart motion. ECG triggering uses the electrical signal of the heart to monitor the progression of the heart motion. The R-wave is used as a reference for starting MRI measurements and a freely selectable delay time can be chosen to measure various stages of the cardiac cycle. This method of motion artifact suppression is useful to get rid off any image blurring due to heart motion. Pulse triggering works in a similar way. The pulse pressure at the fingertip serves as synchronization signal. Motion and flow artifacts are suppressed with pulse triggering. This method is less complex than ECG triggering and facilitates routine
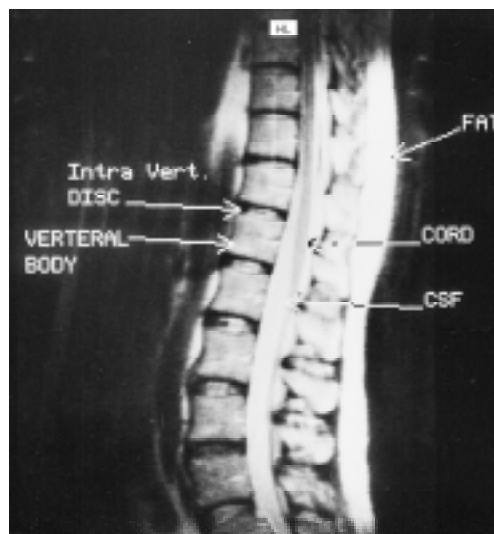

Figure 5 T2 – weighted sagittal image (TR = 2800 ms; TE = 90 ms, FOV = 400 mm) of the whole spine, showing the different anatomy.

examinations of the heart. Recently, the cardiac MR imaging is matured with the development of new techniques to control motion and flow artifacts. It is now possible to acquire quality images of the heart using breath–hold technique. Alternatively, three-dimensional navigator free-breathing technique offers robust respiratory motion compensation, good enough to visualize coronary arteries (Hartnell et al. 1994, Wielopolski et al. 1998). Moreover, with improvements in MR hardware, such as fast gradients and high-sensitivity radio-frequency coils, it is possible to evaluate cardiac morphology, function, and perfusion in a clinical setting. Also, its possible to evaluate myocardial viability information, and even coronary anatomy and flow. Due to excellent soft tissue contrast, MRI also has wide application in musculo-skeletal systems (Edelman et al. 1995, Higgins et al. 1997). MR image characteristics are different for fat, muscle, fibrous structures, nerves and blood vessels that are of considerable interest to orthopedic surgeons and radiologists.

In the past few years, MRI of flow has evolved into a powerful technique to visualize blood flow in vessels. This technique called as magnetic resonance angiography (MRA), which is proved to be a valuable tool for evaluating vascular diseases (Arlert et al. 1996). In addition to its ability to image vascular anatomy, new noninvasive approaches for measuring blood flow have in fact expanded the role of MRI in diagnosing vascular

pathology; for example, cardiac abnormalities and renal blood flow (Van der Wall & de Ross 1991, Arlert et al. 1996). Moreover, it enables the determination of flow velocity, direction, and even the flow profiles within the vessel. The clinical applications of MRA include the visualization of arteriovenous malformations, aneurysms, venous angiograms, carotid occlusion, thoracic vessels and abdominal vessels. Figure 6 shows the MRA of a patient carried out in our laboratory showing the stenosis of both the left and right carotid arteries.

Recently, considerable interest has arisen in the ability of MRI to image and measure molecular diffusion and blood microcirculation (perfusion). Diffusion and perfusion imaging (Le Bihan 1995, Noris 2001) are useful techniques to evaluate anatomic and functional disorders of the brain and other organs. Both methods share some conceptual points in common, however, refer to different physical phenomena. Molecular diffusion is the result of the thermal or Brownian, random translational motion that involves all molecules, while perfusion results from blood delivery to tissuess.

Diffusion-weighted MR imaging (DWMRI or DWI) can be used to map as well as assess and/or quantitate the microscopic motion of water protons in tissues (Le Bihan 1995, Noris 2001). Measuring molecular diffusion may bring several potentially useful new approaches to tissue characterization and functional studies. In tissue, interactions and

Figure 6 MR angiography (MRA) of a patient showing stenosis (arrow) of carotid arteries.

collisions of water molecule with macromolecules and membranes usually limit diffusion, hence, in biological studies the diffusion coefficient value is quoted as apparent diffusion coefficient (ADC). The local environment influences diffusion; for example, in areas of white matter there is greater diffusion along the myelin sheaths than across the myelinated fiber. Therefore, the diffusion of water in tissues is anisotropic; i.e., there are different apparent diffusion coefficients in each direction. In fact, diffusion is a three-dimensional process and the molecular mobility may not be the same in all directions. This anisotropy may result from the physical arrangement of the medium or from asymmetric disposition of obstacles that limit diffusion. In fact, diffusion is a tensor, an array of numbers that describe mobility rates in different directions. Diagonal elements D_{xx}, D_{yy}, and D_{zz} represent molecular mobility in the three directions X, Y, and Z-axis. The non-diagonal elements, such as D_{xy}, D_{xz}, or D_{yz}, show diffusion in one direction is correlated with some molecular displacements in a perpendicular direction. Since molecules can diffuse in all three dimensions, diffusion tensor mapping becomes more powerful. Diffusion imaging is a major advancement in the continuing evolution of MR imaging. It provides contrasts and characterization between tissues at cellular level that may imply differences in function (Le Bihan 1995, Le Bihan et al.2001).

DWI is useful in the early detection and characterization of cerebral ischemia and is ideal technique for stroke management (Le Bihan 1995, Ozscunar & Sorensen 2000, Molko & Chabriat 2001). Figure 7 shows our data on diffusion-weighted image of a patient who had stroke 12 hrs prior to MRI. The infarct region is seen clearly as a hyperintense area, which could not be clearly differentiated in the T2-weighed image. Recently, we have documented through sequential DWI study, the occurrence of several pathological features during the complete cycle of demyelination and remyelination in an animal model of demyelinating lesion (Degaonkar et al. 2002).

Perfusion MRI (PWI) measures blood flow, which is different in many brain and cardiac disorders (Le Bihan 1995, Barbier et al. 2001). In fact, perfusion MR demonstrates the microscopic vascular proliferation (neovascularization)
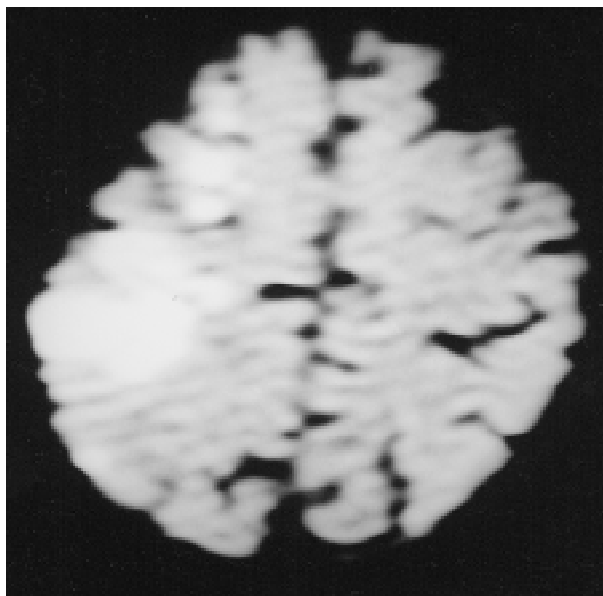
Figure 7 Diffusion-weighted MRI of a patient imaged 12 hrs after stroke. The infarct region in seen as hyper-intense area in the right occipital region.

associated with tumor growth. Tissue perfusion is normally assessed following a dynamic injection of contrast material, gadolinium diethylene triamine pentaacetic acid (Gd DTPA). For example, in cerebral tissues Gd is restricted to the intra-vascular space. Gd being paramagnetic creates microscopic field gradients around the cerebral microvasculature, resulting in a change of T2 relaxation and signal loss. From the amount of signal loss, the concentration of gadolinium in each pixel can be calculated, and a pixel by pixel relative estimate of blood volume can be inferred. Maps of cerebral blood volume (CBV) and CBF can be generated using this information. As a rule, high-grade tumors have higher CBV than low-grade tumors; and CBV values correlate with the grade of vascularity and mitotic activity. Knowledge of tumor vasculature helps improve tumor grading, identify optimal biopsy site in tumors with heterogeneous vascularity, monitor malignant degeneration and treatment efficacy, and differentiate tumor recurrence from radiation necrosis. Similarly, PWI of the myocardium is a useful modality to detect perfusion defects both, at rest and under stress. Contrast enhanced (Gd DTPA) PWI can be reliably used to assess myocardial perfusion in patients with ischemia. The uptake of contrast will be attenuated, in amplitude and rate, in regions of compromised flow.

Yet another advance in MRI is to map changes in brain hemodynamics that correspond to different brain functions. The ability to observe precise anatomical structures and its participation in specific function is due to a technique called 'functional MRI' (fMRI). fMRI provides high resolution, noninvasive report of the neural activity detected by a blood oxygen level dependent (BOLD) signal (Ogawa et al. 1990, Merkle & Ugurbil 1992, Ellerman & Ugurbil 1993). It is based on the increase in blood flow to the local vasculature that accompanies neural activity in the brain. This results in corresponding local reduction in deoxyhemoglobin because, the increase in blood flow occurs without an increase of similar magnitude in oxygen extraction (De Yoe et al. 1994). Since deoxyhemoglobin is paramag-netic, it alters the T2* - weighted MR image signal intensity. Thus deoxyhemoglobin is some times referred to as an endogenous contrast-enhancing agent, and serves as the source of the signal for fMRI. Using an appropriate imaging pulse sequence, human brain functions can be observed without the use of exogenous contrast enhancing agents in many clinical MR scanners (field 1.5 T or greater). Functional activity of the brain determined from the MR signal has confirmed anatomically distinct processing areas in the visual cortex (Fox & Raichle 1986, Belliveau et al. 1992), the motor cortex (Kim et al. 1993, Jagannathan & Raghunathan 1995), and Broca area of speech and language related activities (Hinke et al. 1993). Figure 8 shows the effect of left-hand movement performed by a volunteer (our work); the appropriate cortical activity can be clearly seen near the sulcal wall. The ability to directly observe different brain functions opens an array of new opportunities to advance our understanding of brain organization, as well as a potential new standard for assessing neurological studies and risks (Moonen & Bandettin 2000, Buxton 2001).

MR imaging of nuclei other than proton, such as ^{23}Na and ^{19}F, have also been reported. Such measurements are exacerbated by the low intrinsic sensitivity of these nuclei relative to proton and the low physiological concentrations relative to water. Sodium MRI studies have demonstrated that the method can be useful for monitoring edema development, cerebral redistribution of sodium
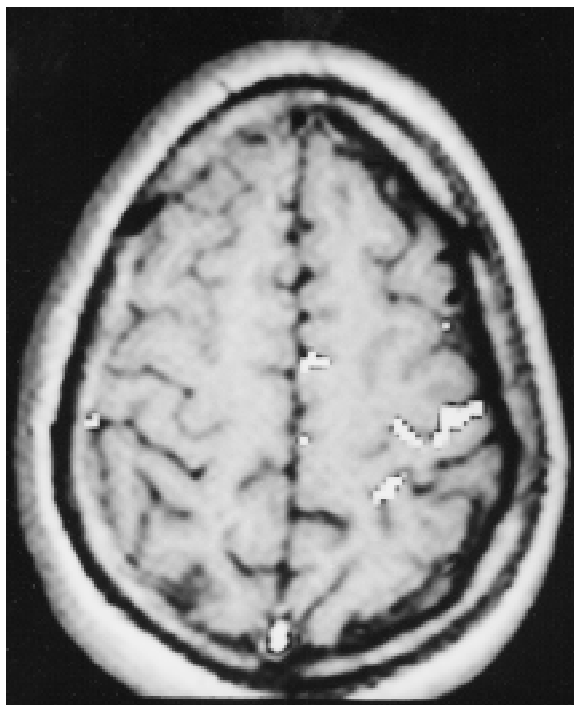
Figure 8 Functional MR image of a volunteer who is carrying out right hand finger movement. The appropriate cortical activity in the left motor area (volunteers left) is shown as hyper intense signal on a T1-weighed MR image. Note: the activation (white spots) that appear on right side of the   image shown is actually the volunteer's left.

following ischemia (Lin et al. 2001) and myocardial infarction (Sandstede et al. 2001). The technique has also been found to be useful to detect early cartilage degeneration (Shapiro et al. 2002). Since there is no MR visible fluorine in human body, the ^{19}F MRI methodology depends on the exogenous addition of a fluorinated material. Perfluorocarbons that label vascular compartments at high concentration have been commonly used, especially in the assessment of vascularity and the kinetics of tissue perfusion (McIntyre et al. 1999).

Recently, studies have shown that inhalation of hyperpolarized (HP) gas allows images of the human lung air spaces by MRI with excellent contrast resolution (Albert et al. 1994, Ebert et al. 1996, Albert et al. 1999, Kauczor et al. 1998, Kauczor 2000, McAdams et al. 2000, Salerno et al. 2001). Conventional proton MRI yields very poor images of the lungs because they are filled with air and contain little water. Gases like ^{3}He or ^{129}Xe, both chemically inert noble gases with spin 1/2, are polarized by optical pumping before inhalation. Nuclear polarization up to 80% is achieved which

corresponds to a huge polarization enhancement or hyperpolarization above the thermal polarizations obtained in standard MRI. The method has immense potential applications in the domain of lung pathology and other perspectives in functional MRI.

MRI in Drug Evaluation

MRI is a useful technique in pharmaceutical and drug research that enables us to understand the pathophysiology of interaction of drugs with tissue *in vivo*. This method allows evaluation of the efficacy of drugs, including *in vivo* concentration determination. In this section, few specific examples of how MRI can be used in drug evaluation are presented.

Cerebral infarction is the major cause of mortality and morbidity in many countries. Despite considerable research efforts, there is presently no generally accepted therapy. MRI has been used to investigate the early pathological events associated with cerebral infarction in animal models, such as unilateral occlusion of the common carotid artery in gerbils (Buonano et al. 1983) or the middle cerebral artery occlusion (MCAo) in animals (Sinha et al. 2001, Gupta et al. 2002). The MCAo model in rats has also been used to test drugs with various mechanisms, aimed at reducing the extent of cellular damage in the acute phase of stroke. These drugs are calcium antagonists, NMDA antagonists, A M PA antagonists, ion channel modulators, anti-inflammatory drugs, etc. In several cases, it was demonstrated that the cytoprotective effects found at 24 or 48h after MCAo persisted up to 14 and 28 days and could in these cases be considered permanent (Sauter et al. 1988, Sauer et al. 1994). Several drugs also showed efficacy when administered after permanent MCAo (Sauter & Rudin 1990).

DWI technique allows a more efficient and accurate measurement of stroke volume in experimental animal models. Recently Qui et al. (Qui et al. 1997) have documented the progression of a focal ischemic lesion in rat brain during treatment with a novel glycine/NMDA antagonist *in vivo* using 3D diffusion weighted MR study. They have documented that the stroke volume had increased by 15% in the control group, in contrast, to the treated group that showed a 40% reduced stroke volume.

Of the several mechanisms of neuronal injury in stroke, free radicals have also been implicated during ischemia reperfusion. Melatonin, a potent antioxidant, has been used in male Wistar rats subjected to 2hr of transient MCAo to study its effect on ischemia (Sinha et al. 2001). Melatonin (10,20 and 40 mg/kg i.p) was administered four times to the animal at the time of MCAo, 1h after MCAo, at the time of re-perfusion and 1h after re-perfusion. In the 20 mg/kg melatonin tested group, the percent ischemic volume in DWI was significantly attenuated when compared to the vehicle treated group. The study indicated that melatonin has neuroprotective action in focal ischemia, which may be attributed to its antioxidant properties (Sinha et al. 2001). Similarly, the effectiveness of adenosine as a neuroprotective agent in MCA occluded rats using DWI has also been demonstrated (Gupta et al. 2002).

Individual tumor physiology is one of the important determinants in the outcome of non-surgical treatments. Parameters such as tumor blood flow, tissue oxygenation and nutrient supply, pH distribution, and bioenergetic status significantly influence tumor response to irradiation, hyperthermia, chemotherapy and a combination of these modalities. In radiotherapy, the efficacy of the treatment depends greatly on the local oxygen concentration, which in turn, is governed by local blood flow. Recently, calcium channel blockers (CCB) have been observed to modify the tumor blood flow in experimental tumors (Wood & Hirst 1989). Diltiazem, belonging to the benzothiazipine group of CCBs, has been shown to protect normal tissues from the lethal and sub-lethal effects of radiation. Recently, Muruganandham et al. (1999) have used gadodiamide contrast enhanced dynamic MRI to investigate the diltiazem induced micro-circulatory changes in tumor and normal muscle of Swiss albino stain A mice. In addition, the MR BOLD contrast method was also used to assess tumor oxygenation status before and after diltiazem administration. The diltiazem plus radiation treated mice showed significant tumor regression and enhanced animal survival. Thus, this study revealed that diltiazem has the potential as an adjuvant in radiation therapy apart from its use in chemotherapeutic drug delivery (Muruganandham et al. 1999).

In modern drug discovery and development, transgenic and knockout animals are important as disease models and for target validation. Several examples of MRI and MRS applications in this field have been reported (Koretsky et al. 1990, Roman et al. 1996). The well-studied system is the creatine kinase, which plays a critical role in the high-energy phosphate (HEP) metabolism (Roman et al. 1996). In transgenic animals with increased expression of creatine kinase in skeletal muscle, no changes in the steady-state HEP levels have been observed, despite increased contractile function.

In vivo Magnetic Resonance Spectroscopy (MRS)

Although MRI is superior in giving information about anatomy and pathology and is a proven clinical diagnostic tool, MRI often lacks biochemical specificity. Another application of clinical MR is *in vivo* MR spectroscopy which is capable of providing biochemical (metabolic) information from a well-defined region of interest of living systems, for example, the human brain (Danielson & Ross 1999). In MRS the data obtained is presented as spectra (see figure 9) and are not represented as images. In, MRI water protons are used to create images, but there are other protons of biologically significant molecules (biochemicals) distributed throughout the human tissues that are not seen in MRI. A small proportion of these molecules is present in sufficient concentrations to produce a measurable MR signal. Because each has a unique frequency (RF) specific to the biochemical itself (called 'chemical shift'), and entirely distinct from the frequency of water protons, a spectrum of tissue chemistry results from particular area of a human organ under investigation. Thus, a MR spectrum is a curve or a plot of the MR signal intensity as a function of MR frequency measured in units of parts per million (ppm) relative to the frequency of a reference compound (see figure 9B vide infra). Each peak in a spectrum derives from a different biochemical present in the tissue and its integrated signal intensity or area is proportional to the concentration of that particular biochemical. For example, a MR spectrum can be used to discriminate healthy tissues from cancerous
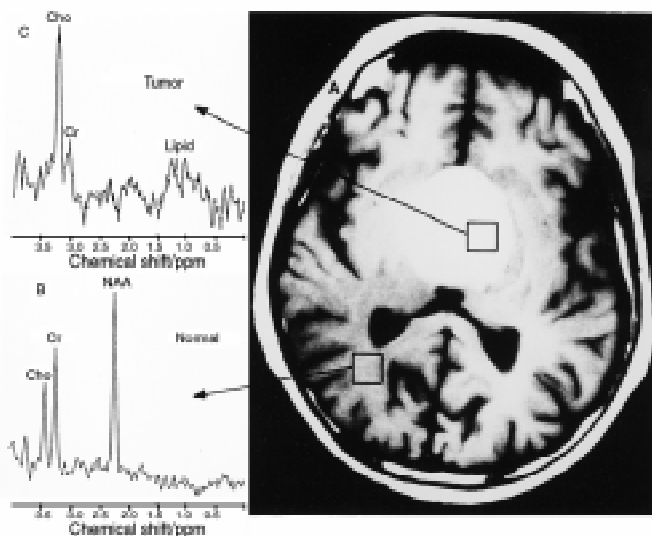
Figure 9 (**A**) T1-weighted axial MR image (TR = 550 ms; TE = 15 ms; slice thickness = 4 mm; FOV = 230 mm) of a patient suffering from a brain tumor (cranio pharyngioma) in the floor of the third ventricle. (**B**) Proton MR spectrum from an 8 ml voxel from the normal position (temporal region) of the brain of the patient (TR = 3000 ms; TE = 135 ms; NS = 256). (**C**) Proton spectrum of the same patient from an 8 ml voxel positioned in the tumor region (TR = 3000 ms; TE = 135 ms; NS = 256).

tissue. This gives MRS the ability to provide insight into the biochemical changes underlying a particular disease. Information that normally requires biopsies (invasive) can now be acquired by MRS non-invasively, *in vivo*. At present, MRS is being used in many areas of cancer research, such as intracranial tumors (Luan & Zhang 1998, Castillo & Kwock 1999), head and neck cancers (Danielsen & Ross 1999), breast cancers (Jagannathan et al. 1998, 1999, 2001), and prostate cancers (Kurhanewicz et al. 2000, Swanson et al. 2001).

Metabolites that are Detected by MRS

MRS can be carried out using different nuclei such as ^{1}H, ^{31}P, carbon (^{13}C), lithium (^{7}Li) and fluorine (^{19}F), etc. ^{31}p MRS provides information about energy status [phosphocreatine (PCr), inorganic phosphate (Pi) and nucleotide phosphates (NTP)], phospholipid metabolites [phosphomonoesters (PME), phosphodiesters (PDE)], intracellular pH and free cellular magnesium concentration. Natural abundance or enriched ^{13}C MRS provides information about glycolysis, gluconeogensis, amino acids and lipids. Water-suppressed ^{1}H MRS shows total choline (TCho), total creatine (TCr),

lipids (Lip), glutamate (Glu), glutamine (Gln), inositols (Ins), lactate (Lac), and N-acetyl aspartate (NAA). ^{7}Li and ^{19}F MRS can be used to study pharmacokinetics.

Figures 10 and 11 depict the metabolic pathways (Scriver et al. 1989, Murray 2000) which have become more relevant since the advancement of *in vivo* MRS. This is because, it is possible to detect certain biochemicals that participate in different metabolic pathways. For example, PCr, NTPs, etc., involved in energy pathways and NAA, TCr, TCho, etc., involved in neurochemical pathways mainly through ^{31}P and ^{1}H MRS, respectively. Figure 10 depicts the major pathways of energy metabolism that occur in cells of the body. Fatty acids and sugars (largely glucose) serve as fuels to provide energy to the cells on oxidation. Glucose after entering the cell, may be either stored as glycogen, or metabolized by glycolytic and oxidative pathways. In the absence of oxygen, glucose may be converted to lactic acid, generating limited amounts of ATP. In the presence of oxygen, the citric acid cycle (or tricarboxylic acid cycle, TCA) metabolizes the metabolic products of glucose or fatty acids within the mitochondria producing CO_2. ATP generated from oxidative phosphorylation is exported to the cytosol where it is used for cellular work and in turn is hydrolyzed. The energy producing reactions of biosynthesis (not shown in the figure), muscle contraction and ion transport are driven by the breakdown (hydrolysis) of high-
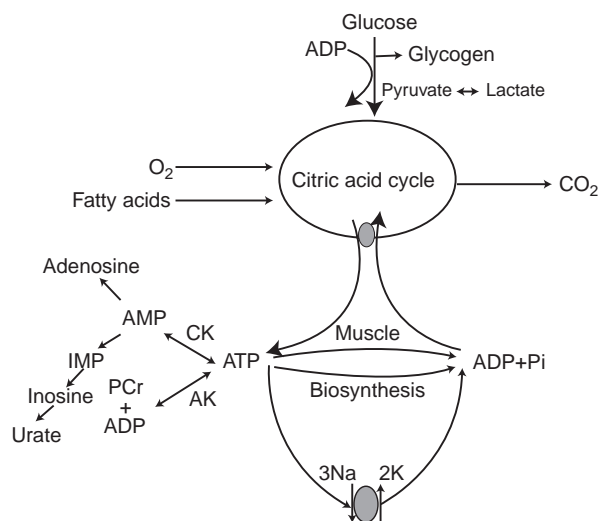

Figure 10 The metabolic pathway showing the energy and neurochemical pathways. The biochemicals (metabolites) shown in bold are detectable by proton and phosphorus MRS.
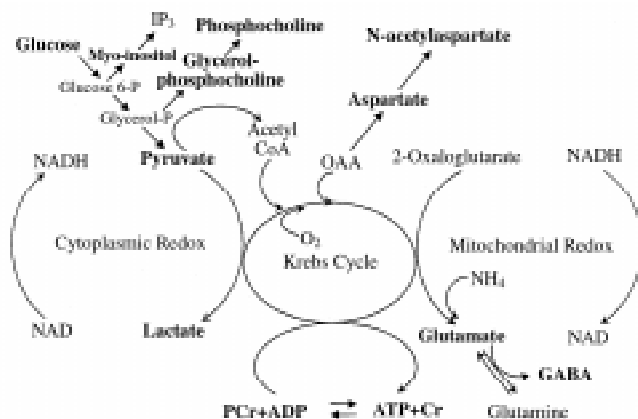
Figure 11 The metabolic pathway observed specifically in brain cells. The biochemicals shown as bold are detectable by proton MRS.

energy phosphate bonds of ATP. Hydrolysis of ATP produces ADP and Pi. In the presence of oxygen, ADP and Pi reenter the mitochondria and are re-synthesized to form ATP. Alternatively, ADP may be subsequently converted to AMP, adenosine, inosine, and ultimately uric acid.

In muscle (skeletal and cardiac) and brain, the enzyme creatine kinase is responsible for generating the storage form of high-energy phosphate, PCr. When sufficient oxygen and fuels are available to facilitate ATP synthesis, abundant amounts of PCr are produced. In time of energy crisis, when hypoxia, ischemia, or cell damage inhibits ATP synthesis, PCr serves to maintain ATP levels so that cellular work can continue. However, if PCr stores are depleted and ATP is not synthesized, ATP concentration will fall to a point at which muscular contraction and ion transport can no longer occur.

Inhibition of the sodium pump causes loss of cellular potassium and increase of cellular sodium, resulting in edema and cell death. Therefore, conditions that impair cell function or viability such as anoxia, ischemia, or tissue damage produce the following events: (a) impairment of ATP synthesis resulting in a fall of PCr and rise of Pi; (b) ultimately, depletion of ATP concentration; and (c) production of lactic acid, resulting in rise of tissue lactate concentration and fall of pH. Restoration of tissue oxygenation leads to a reversal of these events: lactate concentrations fall, and pH returns to control. ATP and PCr concentrations rise while Pi falls. The phosphorous metabolites that are shown in bold in figures 10 and 11 are detectable *in vivo*. In

addition, figure 11 presents the additional biochemical pathways observed specifically in brain cells (Danielsen & Ross 1999). Their linkage with other standard pathways is also shown to give an overview of the whole metabolic activity in brain. The metabolites that can be picked up by ^{1}H MRS in such pathways are presented in bold.

[31]P MR Spectroscopy

In fact, ^{31}P MRS has become the tool of choice to investigate noninvasively energy metabolism in human muscle (Cozzone & Bendahan 1994) and in tumors (Negendank 1992). It is widely used as a technique to measure pH *in vivo* . Studies on human muscle revealed that in normal exercising muscle, the concentration of ATP remains constant while PCr falls and Pi increases (Argov et al. 2000). Intense exercise produces severe intracellular acidosis and changes in pH. During the recovery period PCr gradually increases, Pi and ADP decrease, and pH returns to its rest level. ^{31}P MRS is also used for diagnosis and monitoring of many mitochondrial diseases. The level of PCr/Pi at rest in muscles was lower in mitochondrial myopathy (Arnold et al. 1985). High intracellular pHs in association with the loss of PCr at rest has also been reported in the muscle of patients with muscular dystrophy (Griffiths et al. 1985, Younkin et al. 1987, Kemp et al. 1993). *In vivo* ^{31}P MRS is a useful tool to monitor metabolic changes in disease processes that affect the brain. Reduction in PCr and PDE with increased PME is reported in meningiomas (Newman et al. 1982) and other brain tumors (Hubesch et al. 1989, Heindel et al. 1998, Maintz et al. 2002). ^{31}P MRS has also been used to monitor metabolic changes in brain tumors after radiation and chemotherapy (Segebarth et al. 1989).

Proton MR Spectroscopy

The majority of MRS applications have been on the human brain especially using a proton nucleus. It plays a vital role in the assessment of clinical trials, including the monitoring of new drug therapies. The clinical utility of MRS rests on two important properties. First, the nature and concentration of tissue biochemicals is remarkably consistent, hence a "normal" tissue (e.g. brain) spectrum is readily recognized. Secondly, a particular biochemical is of clinical relevance in healthy and/or diseased state.

Accordingly, abnormal brain MR spectra are readily recognized and classified. Together with the abnormal anatomy and physiology identified by the MRI, MRS gives a more complete picture of disordered metabolism encountered in clinical practice (Danielsen & Ross 1999, Rand et al. 1999, Burtscher & Holtas 2001). Proton MRS is also a useful modality to detect biochemical abnormalities at the molecular level in chronic alcoholics (Jagannathan et al. 1996) and in congenital hypothyroidism (Jagannathan et al. 1998) even before structural damages are apparent in MRI.

In this section, a few examples from the study carried out in our laboratory are presented to show the potential of in *vivo* MRS in actual clinical setting. The transaxial MR image of a patient suffering from brain tumor (cranio pharyngioma) in the floor of the third ventricle is shown in figure 9A. Proton *in vivo* MRS from an 8cc ($20 * 20 * 20$ mm^3) volume (voxel) from the normal posterior temporal region of the brain shows (figure 9B) three major peaks labeled as NAA, Cr and Cho. NAA is an amino acid and is generally considered to be a neuronal marker. It is distributed throughout the cerebral cortex with a concentration in the range of 7–15 mM.

Any change (mainly decrease) of NAA in relation to a healthy brain tissue indicates altered metabolism such as neuronal loss or neuronal death in variety of brain tumors (table 3). The total Cr (with PCr) metabolite appears as a single peak at 3.00 ppm, and is a reliable marker of intact brain 'energy metabolism'. Its normal concentration in human brain is 4.0–5.5 mM. The TCho peak [arising from phosphocholine (PC), glycerophosphocholine (GPC) and free choline] is altered in many disease processes (table 3) and its concentration in the normal brain is approximately 1–2 mM. Myo-inositol (mI), a sugar, appears around 3.54 ppm. It is located in astrocytes where it is recognized as the most important osmolyte, or cell volume regulator. Glutamate and glutamine appear together as a broad complex pattern near 2.3 ppm and is normally denoted as "Glx". Glutamine, like mI, is an astrocyte marker, while glutamate functions as an excitatory neurotransmitter, but obviously has a number of other functions. Lactate is not observed in normal brain and hence its appearance is indicative of altered metabolism; mainly failed oxidative metabolism in the brain (table 3). A proton spectrum of the same patient

Table 3 *Concentration of some brain biochemicals (metabolites) in normal and diseased states*

Biochemical	Increased (↑)	Decreased (↓)
N-Acetyl-aspartate (NAA) (normal 7-15mM)	Axonal recovery e.g. MS; infant development; hyperosmolar states; Canavan's; post head injury.	Hypoxia; anoxia; ischemia; Alzheimer's and other dementia; developmental delay; epilepsy; MS; neoplasm; stroke; lymphoma; tumor; encephalitis; diabetes mellitus; Alexander's; AIDS/HIV.
Creatine (Cr) (normal 4-5 mM)	Trauma (Hyperosmolar response); increase with age.	Hypoxia; stroke; tumor; infant; trauma lymphoma; hyponatremia; toxoplasmosis; PML
Choline (Cho) (normal 1-2 mM)	Trauma; diabetes; neonates; post liver transplant; tumor; chronic hypoxia; stroke; post liver transplant; hypersomolar.	Asymptomatic liver disease; HE; toxoplasmosis; nonspecific dementia; hyponatremia
Lactate (Lac) (normally less then 1 mM)	Hypoxia; anoxia; ICH; near-drowning; stroke; Canavan's; Alexander's; hydrocephalus; lymphoma; toxoplasmosis.	
Lipids (Lip)	Lymphoma; cryptococcoma; active growing tumor; PML; toxoplasmosis; MS; inflammatory diseases.	
myo-inositol (mI) (normally 5 mm)	Alzheimer's Diabetes mellitus Hyperosmolar states; Neonate PML	Chronic HE; stroke Tumor; lymphoma; Hypoxic encephalopathy

from a 8cc voxel from tumor shows (figure 9C) the absence/reduction of the neuronal marker (NAA) and the energy metabolic marker (Cr), while the choline level is seen to be elevated, indicating the presence of a tumor.

Seizures and epilepsies make up a heterogeneous collection of episodes of disturbed cerebral function. In a large number of patients with seizures, MRI demonstrates atrophy and/or high-signal intensity in the affected area. However,a significant number of these patients has normal MRI studies. The use of MRS is suggested in such cases along with DWI investigations. Many reports of single and multi-voxel proton MRS have been reported. Common to all MRS studies is the decrease in NAA in the affected area compared to normal controls that represent neuronal dysfunction and neuronal loss (Achten et al. 1997, Thompson et al. 1998, Jackson & Connelly 1999, Rudkin & Arnold 1999). MRS localizes unilateral seizure foci in concordance with the EEG. In addition, it also demonstrates the presence of high proportion of bilateral abnormalities (Connelly et al. 1994), which can be difficult to observe by other techniques. Observation of elevated lactate has been reported in a limited number of studies (Matthews et al. 1990, Ng et al. 1994). The local increase in lactate can persist for several hours and may be used as a more direct marker of seizure activity (Danielsen & Ross 1999, Rudkin & Arnold 1999). Studies have also demonstrated elevated γ-amino butyric acid (GABA) levels after treatment with vigabration, an anticonvulsant that acts as an irreversible GABA transaminase inhibitor (Rotham et al. 1993, Petroff et al. 1996).

Proton MRS methods have also been extensively used to study acute and chronic functional impairment in multiple sclerosis (MS) which results from multiple mechanisms, including demyelination, conduction block, and axonal injury. The main finding in MS lesions is decreased NAA. However, early increase in Cho and lactate, as well as early transient decrease in Cr can be observed (Arnold 1999, Rudkin & Arnold 1999). Studies using short echo times have shown increased mI and lipid signals (Davie et al. 1994). Recently, sequential proton MRS studies of brain metabolite changes were monitored during a complete pathological cycle of

demyelination and remyelination in experimental demyelinating lesion model of MS (Degaonkar 2002).

Infectious CNS diseases are often the cause of seizures in the tropical countries like India, and these are often caused by cysticercosis or tuberculosis. In the absence of appropriate therapy, the disease can be fatal, and noninvasive differential diagnosis would be of great relevance. In fact, proton MR spectroscopy has been found to be useful in patients where radiological investigations are not specific (Jayasundar et al. 1995, Jayasundar et al. 1999, Gupta et al. 2001, Shukla et al. 2001, Venkatesh et al. 2001). Local temperature in tumors, in addition to influencing a number of normal biological functions such as the protein activity, enzyme mediated reactions, hemoglobin's affinity for oxygen, etc. are also known to play an important role in diseases (Vanda et al. 1990). MRS is an ideal technique to determine the local temperature of tumors noninvasively. For example, even small variations in brain temperature can affect the extent of injury in brain ischemia (Jayasundar & Singh 2001). Therefore, knowledge of local temperature could provide additional information on the pathophysiology of the disease processes to the clinicians. Recently, few papers have described the role of proton MRS to measure tissue pH (Rothman et al. 1997, Pant et al. 1988, Van Sluis et al. 1999).

In our laboratory, the role of *in vivo* MRS in the study of breast cancer was evaluated in 100 patients. The MR image from one patient suffering form infiltrating ducatal carcinoma (IDC) of the breast is shown in figure 12A, while figure 12B is the proton MRS from the normal region of the breast and figure 12C is from the tumor. Significant spectral differences between the normal and tumor portions of the breast is clearly visible. The presence of choline from the tumor can be used as a metabolite marker of malignancy and its level reduces/ disappears in patients treated with neoadjuvant chemotherapy (NACT). Our study revealed that *in vivo* proton MRS has 78% sensitivity and 86% specificity in detecting choline in malignant breast tumors. In comparison, the sensitivity and speci-ficity of dynamic contrast MRI was 30-95% and 60 - 80%, respectively (Haywang-Kobrunner et al. 1997). Observation of choline before treatment and its disappearance (or reduction) after treatment
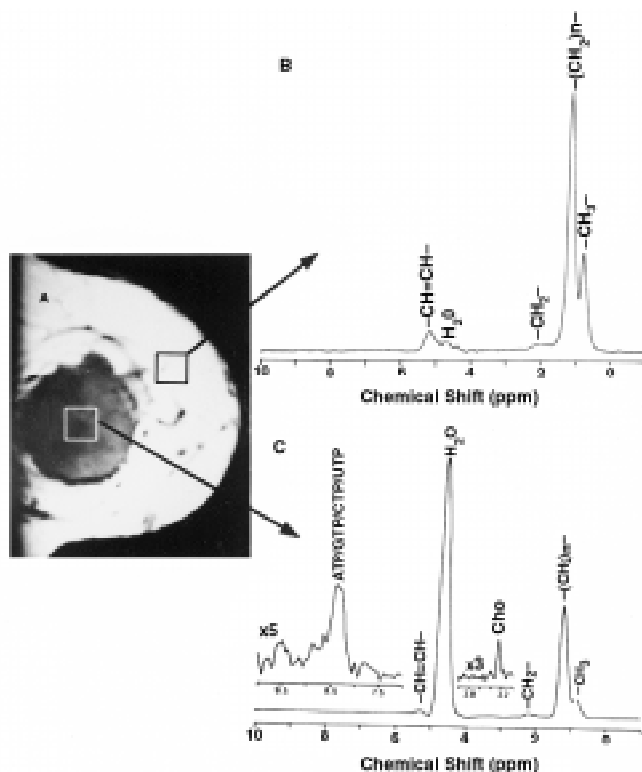
Figure 12 (**A**) T 1 – weighted sagittal MR image showing the tumor of a patient suffering from infiltrating ductal carcinoma (IDC) of the breast (slice thickness = 5 mm; TR = 600 ms; TE = 15 ms); (**B**) Volume localized proton MR spectrum from an 8 ml voxel positioned in the normal position of the breast of the same patient (TR = 3000 ms; TE = 135 ms; NS = 32); (**C**) Volume localized proton MR spectrum from an 8 ml voxel from the tumor position of the same patient (TR = 3000 ms; TE = 135 ms; NS = 64).

serve as a useful indicator of response to treatment (Jagannathan et al. 1998, 1999, 2001). Accurate assessment of tumor response to treatment by MRS helps in selecting patients for breast conservation. Such studies have shown that *in vivo* MRS is a beneficial, noninvasive technique to assess the response of tumors to different drug treatments. In general, monitoring the levels of various tumors metabolites both prior to surgery/therapy and after surgery/therapy helps the patient's therapeu-tic management (Tomi et al. 1997, Jagannathan et al. 1998, 1999, 2001). It is also a useful modality to monitor efficacy of different drugs as well as testing of new drugs.

Spectroscopic Imaging (SI) or chemical shift Imaging (CSI) is a technique that combines features of both imaging and spectroscopy (Brown et al. 1982, Maudsley et al. 1983). It is a method for collecting spectroscopic data from multiple adjacent voxels covering a large VOI in a single measurement. Spatial localization is done by phase encoding in one (1D CSI), two (2D CSI), or three dimensions (3D CSI). The sequences used for SI are similar to a MR imaging sequence, but with no readout gradient applied during data collection. The presentation of the localized spectral data can be examined in different ways: as single spectra related to individual voxels, as spectral maps, or as metabolite images. In fact, both the spectral maps and metabolite images may be over laid on conventional MR images. CSI is an efficient means for comparing spectra from voxels containing different tissue types. For example, in the case of focal diseases, spectra from a lesion are compared to spectra from normal brain tissues, and heterogeneous metabolic distributions within the lesion may also be investigated. A number of applications of SI technique in the study of several brain pathologies and breast cancers have been reported (Mukherji 1998, Danielsen & Ross 1999, Doyle et al. 1999, Bernasconi et al. 2002).

1Fluorine (^{19}F) MR Spectroscopy

Fluorine, which is 100% naturally abundant, has a sensitivity of 83% to that of ^1H and has relatively a short T1. It is almost entirely absent in the human body and hence a perfect tracer for NMR studies. The only fluorine signal that will be detected comes from the fluorine that is deliberately introduced before the measurement. Many drugs, including numerous psychoactive agents have fluorine as a part of their molecular structure and hence can be detectable by *in vivo* MRS. In addition, *in vivo* ^{19}F MRS can also be used to study the metabolism and pharmacokinetics of these fluorinated drugs in human liver in different combination regimens.

5-fluorouracil (5-FU) and other fluoropyri-midines are anti-neoplastic agents that are widely used either singly or concomitantly in the treatment of human cancers, especially of the gastrointestinal tract, breast and ovary. The metabolism of these drugs has been extensively studied. Figure 13 shows the pathway of 5-FU metabolism (Heidelberger et al. 1983). The catabolic (detoxi-fication) pathway of 5-FU involves hydrogenation and opening of the pyrimidine ring, resulting in α-fluoro-β-ureidopropionic acid and final products, α-fluoro-β-alanine (FBAL), fluoride ion (F⁻), carbon

dioxide, and ammonia. The liver remains the major site for catabolism of 5-FU, since the activity of the enzyme dihydrouracil dehydrogenase is the highest in the liver.

To increase the response rate of 5-FU, other agents are co-administered to modulate the efficacy of 5-FU. Methotrexate (4-amino, 4-deoxy, N-10-methyl pteroylglumaic acid) is one such modulator that binds tightly but reversibly to its target enzyme dihydrofolate reductase, leading to a cessation of de novo purine synthesis. Other modulators that are commonly used are leucovorin and levamisole. The efficacy of these treatment regimens can be assessed by *in vivo* ^{19}F MRS. Numerous studies of 5-FU metabolism in animal models (Stevens et al. 1984, Sijens et al. 1999) and in humans (Wolf et al. 1987, Wolf et al. 1990, and Mohanakrishnan et al. 1999) are reported. The modulation by an effector drug is actually monitored by measuring changes in 5-FU half-life or the time constant ($t_{1/2}$) for the formation of its catabolite, FBAL using *in vivo* ^{19}F NMR examination in the liver.

Figure 14 shows our data on the sequential ^{19}F NMR spectra carried out on a patient with breast cancer (Mohanakrishnan et al. 1999). The initial spectrum recorded in the first 3.5 minutes at the onset of drug administration has only a single peak at about 0 ppm due to 5-FU. In the second spectrum
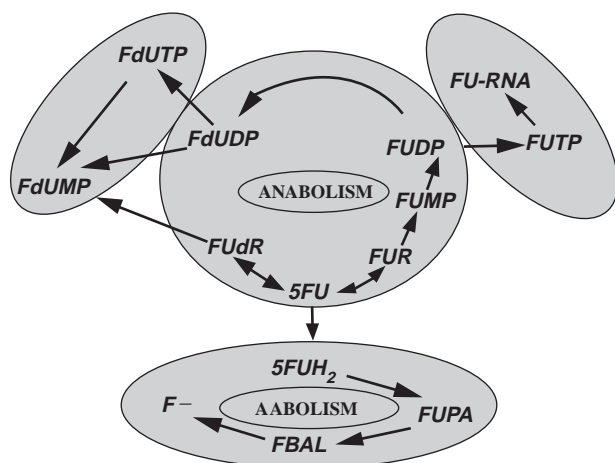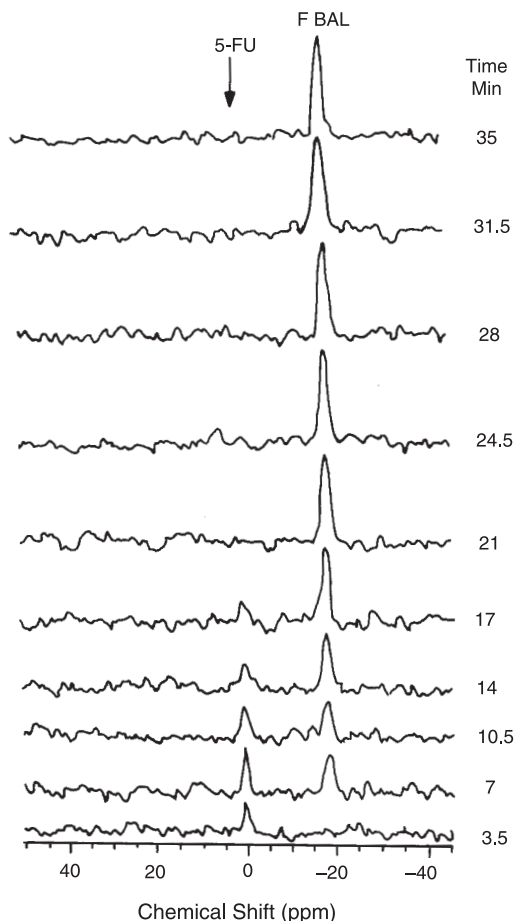

Figure 14 Stacked *in vivo* ^{19}F MR spectra at 60.1 MHz as a function of time from the liver of a breast cancer patient following the bolus infusion of 5-FU two hours after methotrexate administration.

recorded after 7 minutes, the signal intensity of this peak increases and, another signal appears at about -19 ppm that is assigned to FBAL on the basis of its relative chemical shift. The 5-FU signal intensity decreases and FBAL intensity increases with time in subsequent spectra recorded at various timings as shown. At about 21 minutes, no 5-FU signal is visible. The apparent time constant ($t_{1/2}$) for the disappearance of 5-FU resonance and the appearance of FBAL in liver are 15 ± 1.6 min and 25 ± 2.2 min, respectively. The $t_{1/2}$ for 5-FU in liver among 9 patients studied by us under different combination regimens of modulators varied between 5 and 17 min and this agrees with the $t_{1/2}$ for 5-FU in blood. The $t_{1/2}$ values of 5-FU trapped in tumors ranged between 20 and 78 minutes. In spite of the increase in $t_{1/2}$ values for intratumoral 5-FU, fluorinated nucleoside/nucleotide signals were not detected. It

Figure 13 Pathways of 5-FU metabolism. The different products of the metabolic pathways are: 5 - FU (5-fluorouracil); FUR (5-fluorouridine); FUdR (5-fluoro-2'-deoxyuridine); F U M P, FUDP, FUTP (5-fluorouridine -5$_1$' - mono-, di-, triphosphate); FdUMP, FdUDP, FdUTP, (5-fluoro-2'-deoxyuridine -5' - mono-, di-, triphosphate); 5FUH$_2$ (5, 6-dihydro-5-fluorouracil); FUPA (± - fluoro - ^{2}-ureidopropionic acid); FBAL (± - fluoro - ^{2}-alanine); F$^-$ (fluoride ion).

may be possible that 5-fluoro-2'-deoxyuridine 5' monophosphate (FdUMP) formed is rapidly incorporated into DNA/RNA and the fluorine signals from these macromolecules are too broad to detect. Based on the results obtained from a number of patients who were receiving 5-FU and additional chemotherapeutic agents such as methotrexate, leucovorin or levamisole, it is concluded that the modulators of 5-FU do not significantly lengthen the time constant for the disappearance of 5-FU from the liver (Mohanakrishnan et al. 1999). ^{19}F MRS has also been used to study the concentration level in the brain of antipsychotic drugs such as trifluoperazine and fluphenazine and the antidepressant fluoxetine (Durst et al. 1990, Renshaw et al. 1992, Komoroski et al. 1995).

Lithium (^{7}Li) MR Spectroscopy

The isotope ^{7}Li has a spin 3/2, receptivity about 27% of ^{1}H, and is a relatively attractive nucleus for NMR studies. It typically gives a single narrow line in most biological systems arising from the Li cation, in both the intracellular and extracellular environments. Lithium salts are used with considerable success in alleviating or preventing both depressive and manic recurrences of manic-depressive illness. There is a considerable interest on its clinical effects, pharmacokinetics and mechanism of action. However, its mechanism of action remains unknown. Patient monitoring relies on measurement of the Li level in serum and the range 0.5-1.2 mmol/L considered to be the optimum level and those greater than 2.0 mmol/L, are toxic. Of course, serum levels may not reflect brain concentrations, which might be expected to relate more closely to clinical response. Patient monitoring and elucidation of Li biochemistry *in vivo* are difficult due to lack of suitable methods to follow the distribution, concentration and physical state, for example, degree of ion binding, etc., of Li in various organs. There is no known method for following Li concentration *in vivo* in humans available except NMR spectroscopy although a neutron activation method has been proposed. Renshaw and co-workers have extensively studied the application of ^{7}Li NMR *in vivo* spectroscopy (Gonzalez et al. 1993).

Figure 15 shows the results obtained by Komoroski et al. (1990) of a patient suffering from manic-depressive illness with an episode of hypomania. The patient was under Li therapy (900 mg/day of Li_2CO_3 in three doses). The serum level of Li rises to about 0.75 mmol/L in 8 days, and then drops to 0.6 mmol/L. The drop occurred during a brief release of the patient from the hospital indicating the suspicion of noncompliance with therapy during this period. The Li level in muscle rises steadily through the seventh day, dropping precipitously thereafter. The brain Li level rose more rapidly than that for muscle initially, then more slowly thereafter. Thus, it appears that the Li level in muscle more closely follows the serum level. Several other workers have also noticed that the Li level in brain is about half those in serum (Komoroski et al. 1990, Kato et al. 1992). Gonzalez et al. (Komoroski et al. 1993) have measured the Li level in the brain by computerized morphometric analysis and compared it that obtained from muscle, cerebrospinal fluid, and blood obtained using MRS. The important issue is the compartmentation of the Li ion *in vivo* and ignoring the different cell types, the ratio of intracellular-to-extracellular Li concentration is not known in brain. Li presumably works intracellularly in the brain and about 80% of the volume of the brain is intracellular; the intracellular concentration may be substantially lower than extra cellular concentration, as is the case for Na. Thus, the *in vivo* Li signal may primarily represent non active Li, however, it is very difficult to find out the ratio of the intracellular-to-extracellular Li concentrations (Komoroski 1993). The compartmentation issue can probably be solved by *in vivo* perfusion studies of cultured cells (Komoroski 1993).
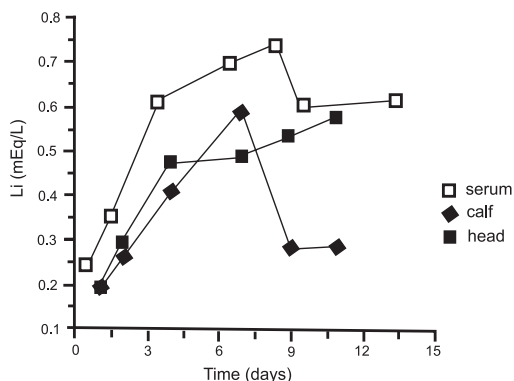

Figure 15 Pharmacokinetics of lithium by ^{7}Li NMR in serum, brain and calf muscle of a patient suffering from bipolar illness.

Conclusions

MR due to its multiplanar imaging capability, high spatial resolution, excellent soft tissue contrast, and the absence of ionizing radiation is well established as a tool in clinical, experimental and biological research. It covers a broad range of applications from fast noninvasive anatomical measurements, to studies on tissue physiology and metabolism. Since it is noninvasive, studying chronic diseases both in humans and animals has several advantages for repeated monitoring of disease progression and therapy response. The method is also highly desirable when studying transgenic and knockout animals. A major use of MR in experimental animal research is the possibility of directly linking pre-clinical to clinical findings. MR can also be used for pharmacodynamic studies in humans to assess whether new compounds are exerting the same pharmacological effects in patients as in animals. Such studies will serve and guide the dose selection for the extensive and expensive clinical efficacy trials. As MR technology matures, the technological limits on the achievable scanning speed and pixel resolution are rapidly approaching the limits imposed by the laws of physics.

Due to the high natural abundance of hydrogen, and its ubiquity in all *in vivo* metabolites, it has been the focus of many clinical MRS studies. The potentially powerful feature of *in vivo* MRS is the ability to measure endogenous metabolites noninvasively as well as changes in tissue metabolism for example, by ^{1}H or ^{31}P MRS monitoring of endogenous metabolites (such as energy metabolism, acidosis, etc.). The technique can also be used for measuring the distribution, and pharmacokinetics of drug *in vivo,* in both humans and animal systems. MRS is currently employed for clinical investigation in many sites around the world, including India. The sensitivity and specificity of *in vivo* MRS for several disease patterns, particularly for small lesions, need to be improved before MRS can be incorporated into clinical practice. Presently, MRS is acting as a complementary tool to histology, mammography and other accepted techniques. However, once MRS becomes established for clinical use unambiguously in one disease, it can be expected that the available technology will be more rapidly be applied to other diseases. In fact, MRS already has great clinical impact in the localization of foci and brain damage in epilepsy and represents a valuable complement to conventional imaging techniques such as CT and MRI. The ability to perform MRI and MRS noninvasively in the same setting with the same equipment with out the injection of radioactive isotopes or blood sampling provides a considerable advantage in patient care.

Future of MR

The future is incredibly optimistic for MR in clinical and experimental research. In less than twenty five years of its induction as a diagnostic modality in clinical radiology, amazing changes have taken place in generating fast high-resolution images with thinner slices, noninvasive brain functionality, etc. MRI has also been developed as a powerful tool to guide interventional procedures in clinical medicine. Designs of new open magnet systems allow improved patient access for MR-guided interventional procedures with the use of MR-compatible needles and catheters. Applications of this interventional MRI include aspiration cytology, chemoablation, cryoblation, etc. The new generation high field strengths MR operating at 3 and 4 Tesla would enable greater detection sensitivity and increased chemical shift dispersion especially for MRS. MR spectroscopy still provides more challenges and can be expected to expand to other clinical areas such as therapy monitoring. MRS, whether it can answer several diagnostic challenges above and beyond MRI, SPECT, PET, and CT will depend on further clinical studies and future technical developments. The future of MR is very bright. The rapid development of new and exciting research will soon provide a virtually limitless ability to accurately diagnose and provide better treatment for patients. This would understandably be a remarkable achievement in medicine made possible through ingenious use of physics.

References

Achten E, Boon P, Van de, Kerckhove T, Caemaert J, De Reuck J and Kunnen M 1997 Value of single voxel proton MRS in temporal lobe epilepsy; *AJNR Am. J. Neuroradiol.* **18** 1131–1139

Ackerman J J H, Grove T H, Wong G G, Gadian D G and Radda G K 1980 Mapping of metabolites in whole animals by ^{31}P NMR using surface coils; *Nature* **283** 167–170

Albert M, Cates G D, Driehys B, Happer W, Saan B, Springer C S Jr. and Wizhaia A 1999 Biological Magnetic Resonance imaging using laser-polarized ^{129}Xe; *Nature* **370** 199–201

Andrew E R, Bottomley P A, Hinshaw W S, Holland G N, Moore W S and Simoraj C 1977 NMR images by the multiple sensitive point method: application to larger biological systems; *Phys. Med. Biol.* **22** 971–974

Argov Z, Lofberg M and Arnold D L 2000 Insights into muscle diseases gained by phosphorus magnetic resonance spectroscopy; *Muscle & Nerve* **23** 1316–1334

Arlert I P, Bougertz G N and Manchal G 1996 *Magnetic Resonance Angiography* (Berlin: Springer)

Arnold D L, Taylor D J and Radda G K 1985 Investigation of human mitochondrial myopathies by phosphorus magnetic resonance spectroscopy; *Ann. Neurol.* **18** 189–196

Barbier E L, Lamalle L and Decorps M 2001 Methodology of brain perfusion imaging; *J. Magn. Reson. Imaging* **13** 496–520

Belliveau J W, Kennedy D N, Mckinstry R C, Buchbinder B R, Weisskoff R M, Cohen M S, Vevea J M, Brady T J and Rosen B R 1992 Functional mapping of the human visual cortex; *Science* **254** 716–719

Bernasconi A, Tasch E, Cendes F, Li L M and Arnold D L 2002 Proton magnetic resonance spectroscopic imaging suggests progressive neuronal damage in human temporal lobe epilepsy; *Prog. Brain Res.* **135** 297–304

Brown T R, Kincaid B M and Ugurbil K 1982 NMR chemical shift imaging in three dimensions; *Proc. Natl. Acad. Sci. USA* **79** 3523–3526

Buonano F S, Pykett I L, Brady T J, Vielma J, Burt C T, Goldman M R, Hinshaw W S, Pohost G M and Kistler J P 1983 Proton NMR imaging in experimental ischemic infarction; *Stroke* **14** 173–177

Burt C T, Glonek T and Barany M 1976 Analysis of phosphate metabolites, the intracellular pH, and the state of adenosine triphosphate in intact muscle by phosphorus nuclear magnetic resonance; *J. Biol. Chem.* **251** 2584–2591

Burtscher I M and Holtas S 2001 Proton MR spectroscopy in clinical routine; *J. Magn. Reson. Imaging* **13** 560–567

Buxton R (ed) 2001 *An Introduction to Functional Magnetic Resonance Imaging, Principles and Techniques.* (Cambridge University Press, London)

Castillo M and Kwock L 1999 Clinical application of proton MR spectroscopy in the evaluation of common intracranial tumors; *Top. Magn. Reson. Imaging* **10** 104–113

Cozzone P J and Bendahan D 1994 ^{31}P NMR spectroscopy of metabolic changes associated with muscle exercise: physiopathological applications; in *NMR in Physiology and Biomedicine* 389–403

Damadian R 1971 Tumor detection by nuclear magnetic resonance; *Science* **171** 1151–1153

Danielsen E R and Ross B 1999 *Magnetic Resonance Spectroscopy Diagnosis of Neurological Diseases* (New York: Marcel Dekker)

Davie C A, Hawkins C P, Barker G J, Brennan A, Tofts P A, Miller D H and McDonald W I 1994 Serial proton magnetic resonance spectroscopy in acute MS lesions; *Brain* **117** 49–58

De Yoe E A, Bandettini P, Neiz J, Miller D and Winans P 1994 Functional magnetic resonance imaging of (fMRI) of the human brain; *J. Neurosci. Methods* **54** 171–187

Degaonkar M N, Khubchandani M, Dhawan J D, Jayasundar R and Jagannathan N R 2002 Sequential proton MRS study of brain metabolite changes monitored during a complete pathological cycle of demyelination and remyelination in a lysophosphatidyl choline (LPC) – induced experimental demyelinating lesion model; *N M R Biomed.* **15** 293–300

——, Jayasundar R and Jagannathan N R 2002 Sequential diffusion – weighted magnetic resonance imaging study of lysophosphatidyl choline induced experimental demyelinating lesion; An animal model of multiple sclerosis; *J. Magn. Reson. Imaging* **16** 153–159

Doyle V L, Barton S J, and Griffiths J R 1999 ^{31}P and ^{1}H MRS of human cancer; *Curr. Sci.* **76** 772–776

Duerinckx A J 1999 Coronary MR angiography; *Radiol. Clin. N. Am.* **37** 273–318

Durst P, Schuff N, Crocq N A, Mokrani M C and Macher J P 1990 Noninvasive *in vivo* detection of a fluorinated neuroleptic in the human brain by ^{19}F NMR spectroscopy; *Psychiatry Res. Neuroimaging* **35** 107–114

Ebert N, Grossman J, Heil W, Otten W E, Sarkar R, Leduc M, Bachest P, Schad M V L R and Thelen M 1996 Nuclear magnetic resonance image with hyper polarized helium; *Lancet* **147** 1297–1299

Edelman R R, Hesselink J R and Zlatkin M B 1995 *Clinical Magnetic Resonance Imaging* (2nd edn) (Philadelphia: W B Saunders)

——, Wielopolski P and Schmitt F 1994 Echo–planar MR imaging; *Radiology* **192** 600–612

Ellerman J M and Ugurbil K 1993 Functional brain mapping by blood oxygenation level–dependent contrast magnetic resonance imaging; *Biophys. J.* **64** 803–812

Fayad Z A and Fuster V 2000 Characterization of atherosclerotic plaques by magnetic resonance imaging; *Ann. NY. Acad. Sci.* **902** 172–186

Fox P T and Raichle M E 1986 Focal physiological uncoupling of cerebral blood flow and oxidative metabolism during somatosensory stimulation in human subjects; *Proc. Natl. Acad. Sci. USA* **83** 1140–1144

Geis R, Hendrick R E, Lee S, Raymond J G, Edward, Hendrick R, Sven Lee B S, Davis K A and Thickman D 1989 White matter lesions: role of spin density in MR imaging; *Radiology* **170** 863–868

Gonzalez R G, Guimaraes A R, Sachs G S, Rosenbaum J F, Garwood M and Renshaw P F 1993 Measurement of human brain lithium *in vivo* by MR spectroscopy; *Am. J. Neuroradiol.* **14** 1027–1037

Griffiths R D, Cady E G, Edwards R H and Wilkie D R 1985 Muscle energy metabolism in Duchenne dystrophy studied by ^{31}P NMR: Controlled trial show no effect of allopurinal or ribose; *Muscle & Nerve* **8** 760–767

Gupta R K, Vatsal D K, Husain N S, Prasad K N, Roy R, Kumar R, Jha D and Husain M 2001 Differentiation of tuberculous from pyogenic brain abscesses with *in vivo* proton MR spectroscopy and magnetization transfer MR imaging; *AJNR Am. J. Neuroradiol.* **22** 1503–1509

Gupta Y K, Singh K, Choudhary G and Jagannathan N R 2002 Protective effect of adenosine against neuronal injury induced by middle cerebral artery occlusion as evident by diffusion weighted imaging; *Pharm. Biochem. Behav.* **72** 569–572

Hartnell G G, Finn J P, Zenni M, Cohen M C, Dupuy D E, Wheller H G and Longmaid H E 1994 MR imaging of the thoracic aorta: Comparison of spin-echo angiographic and breathhold techniques; *Radiology* **191** 697–704

Haywang-Kobrunner S H, Viehuray P, Heining A and Kuchler C 1997 Contrast enhanced MRI of the breast; accuracy, value, controversies, solutions; *Eur. J. Radiol.* **24** 94–108

Heidelberger C, Dannenberg P V and Moran R G 1983 Fluorinated pyrimidines and their nucleosides; *Adv. Enzymol.* **54** 57–119

Heindel W, Heiss WD, Buntie J, Herholz K, Glathe S and Jeske J Comparison of ^{31}P MRS and FDG–PET in human brain tumors (abstract) 1988 Society of magnetic resonance in medicine.; *Seventh Annual Meeting San Francisco* **2** 717

Higgins C B, Hricak H and Helms A 1997 *Magnetic Resonance Imaging of the Body* (3rd edn) (Philadelphia: Lippincot –Raven)

Hinke R M, Hu X, Stillman A E, Kim S G, Merkle H, Salmi R and Ugurbil K 1993 Functional magnetic resonance imaging of Broca's area during internal speech; *Neuro. Rep.* **4** 675–678

Hinshaw W S, Bottomley P A and Holland G N 1977 Radiographic thin section image of the human wrist by nuclear magnetic resonance; *Nature* **270** 722–723

Hoult D I, Bushy S J W, Gadian D G, Radda G K, Richards R E and Seeley P J 1974 Observation of tissue metabolites using ^{31}P nuclear magnetic resonance; *Nature* **252** 285–287

Hubesch B, Marinier D S, Hetherington H, Twieg D B and Weiner M W 1989 ^{31}P MR studies of human brain; *Invest. Radiol.* **24** 1039–1042

Jackson G D and Connelly A 1999 New NMR measurements in epilepsy. T2 relaxometry and magnetic resonance spectroscopy; *Adv. Neurol.* **79** 931–937

Jagannathan N R 2001 *MR Imaging and Spectroscopy in Pharmaceutical and Clinical Research* (New Delhi: Jaypee Brothers)

———, Desai N G and Raghunathan P 1996 Brain metabolite changes in alcoholism: An *in vivo* proton magnetic resonance spectroscopy [MRS] study; *Magn. Reson. Imaging* **14** 553–557

———, Kumar M, Raghunathan P, Coshic O, Julka P K and Rath G K 1999 Assessment of therapeutic response of human breast carcinoma using *in vivo* volume localized proton magnetic resonance spectroscopy; *Curr. Sci.* **76** 777–782

———, ———, Seenu V Coshic O Dwivedi S N Julka P K Srivastava A and Rath G K 2001 Evaluation of total choline from *in vivo* volume localized proton MRS and its response to neoadjuvant chemotherapy in locally advanced breast cancer; *Br. J. Cancer* **84** 1016–1022

———, Meenakshi Singh, Govindaraju V, Raghunathan P, Julka P K and Rath G K 1998 Volume localized *in vivo* proton MR spectroscopy of breast carcinoma; variation of water fat ratio in patients receiving chemotherapy; *NMR Biomed.* **11** 414–422

——— and Raghunathan P 1995 Task activation of the human brain studied in real time by functional MR imaging; *Curr. Sci.* **69** 448–451

———, Tandon N, Raghunathan P and Kochupillai N 1998 Reversal of abnormalities of myelination by thyroxine therapy in congenital hypothyroidism: localized *in vivo* proton magnetic resonance (MRS) spectroscopy; *Dev. Brain Res.* **109** 179–186

Jayasundar R and Singh V P 2001 *In vivo* temperature measurements in brain tumors using proton MR spectroscopy; *Neurology (India)* **84** 1016–1022

———, Banerji A K and Raghunathan P 1995 Proton MRS similarity between CNS non-Hodgkin's lymphoma and intracranial tuberculoma; *Magn. Reson. Imaging* **13** 489–493

———, Singh V P, Jain P, Raghunathan P and Banerji A K 1999 Inflammatory granulomas: evaluation with proton MRS; *NMR Biomed.* **12** 1-6

Kato T, Takahashi S and Inubushi T 1992 Brain lithium concentration by ^{7}Li and ^{1}H magnetic resonance spectroscopy in bipolar disorder; *Psychiatry Res. Neuroimag* **45** 53-63

Kauczor H U 2000 Current issues in hyperpolarized gases in MRI: biomedical investigations and clinical applications; *NMR Biomed.* **13** 173–175

———, Surkau R and Roberts T 1998 MRI using hyperpolarized noble gases; *Eur. J. Radiol.* **8** 820–827

Kemp G J, Taylor D J, Dunn J F, Frostick S P and Radda G K 1993 Cellular energetic of dystrophic muscle; *J. Neurol. Sci.* **116** 201–206

Kim S A, Ashe J, Hendrich K, Ellerman J M, Merkle H, Ugurbil K and Georgopoulos A P 1993 Functional magnetic resonance imaging of motor cortex: hemispheric asymmetry and handedness; *Science* **261** 615–617

Komoroski R A 1993 Measurements of psychoactive drugs in the human brain *in vivo* by MR spectroscopy; *Am. J. Neuroradiol.* **14** 1038–1042

———, Newton J E O, Walker E, Cardwell D, Jagannathan N R, Ramaprasad S and Sprigg J 1990 *In vivo* Lithium-7 NMR spectroscopy of humans; *Magn. Reson. Med.* **15** 347–356

———, Newton J E O, Karson C, Cardwell D and Sprigg J 1995 Deduction of psychoactive drugs *in vivo* in humans using ^{19}F NMR spectroscopy; *Biol. Psychiatry* **29** 711–714

Koretsky A P, Brosnan M J, Chen L, Chen J and Van Dyke T 1990 NMR determination of creatine kinase expressed in liver of transgenic mice: Determination of free ADP levels; *Proc. Natl. Acad. Sci. USA* **87** 3112–3116

Kurhanewicz J, Vigneron D B, Males R G, Swanson M G, Yu K K and Hricak H 2000 The prostate: MR imaging and spectroscopy, Present and future; *Radiol. Clinics N. Am.* **38** 115–138

Lauterbur P C 1973 Image formation by induced local interaction: examples employing nuclear magnetic resonance; *Nature* **242** 190–191

Le Bihan D 1995 *Diffusion and Perfusion Magnetic Resonance Imaging* (New York: Raven Press)

Le Bihan D, Mangin J F, Poupon C, Clark C A, Pappata S, Molko N and Chabriat H 2002 Diffusion tensor imaging: concepts and applications; *J. Magn. Reson. Imaging* **13** 534–546

Lin S P, Song S K, Miller J R, Ackerman J J and Nei J J 2001 Direct, longitudinal comparison of ^{1}H and ^{23}Na MRI after transient focal cerebral ischemia; *Stroke* **32** 925–932

Luan W and Zhang J 1998 *In vivo* hydrogen-1 MRS study of human intracranial tumors; *Clin. Med. J (Engl.)* **111** 56–58

Maintz D, Heindel W, Kugel H, Jaeger R and Lackner K J 2002 ^{31}P MR spectroscopy of normal adult human brain and brain tumors; *NMR Biomed.* **15** 18–27

Mansfield P 1977 Multiplannar image formation using NMR spin echoes; *J. Phys.* **C10** L55–L58

——— and Maudsley A A 1976 Planar and line-scan spin imaging by NMR; Proc. *XIXth Congress Ampere, Heidelberg* 247–252

Matthews P M, Andermann F and Arnold D L 1990 A proton magnetic spectroscopy study of focal epilepsy in humans; *Neurology* **40** 985–989

Maudsley A A, Hilal S K, Perman W P and Simon H E 1983 Spatially resolved high-resolution spectroscopy by four dimensional NMR; *J. Magn. Reson.* **51** 147–152

McAdams H P, Hatabu H, Donnelly L F, Chen O, Tadamura E and MacFall J R 2000 Novel techniques for MR imaging of pulmonary air spaces; *Magn. Reson. Imaging Clin. N. Am.* **8** 205–219

McIntyre D J O, Mccoy C L and Griffiths J R 1999 Tumor oxygenation measurements by ^{19}F magnetic resonance imaging of perfluorocarbons; *Curr. Sci.* **76** 753–762

Merkle H and Ugurbil K 1992 Intrinsic signal changes accompanying sensory stimulation: Functional brain mapping using MRI; *Proc. Natl. Acad. Sci.* **89** 5951–5955

Mohanakrishnan P, Hutchins L, Nauke S, Sprigg J, Cardwell D, Williamson M R, Komoroski R A and Jagannathan N R 1999 Metabolism of 5-fluorouracil in human liver. An *in vivo* ^{19}F NMR study; *Curr. Sci.* **76** 677–680

Molko N and Chabriat H 2001 Diffusion tensor imaging: concepts and applications; *J. Magn. Reson. Imaging* **13** 534–546

Monelfe C 1992 *Imaging of the Spine and Spinal Cord* (New York: Raven Press)

Moon R B and Richards J H 1973 Determination of intracellular pH by ^{31}P magnetic resonance; *J. Biol. Chem.* **248** 7276–7278

Moonen C T W and Bandetti P A (eds) *2000 Functional Magnetic Resonance Imaging* (Springer Verlag, Heidelberg)

Mukherji S K 1998 *Clinical Applications of Magnetic Resonance Spectroscopy* (New York: Wiley-Liss)

Murray R K, Granner D K, Mayer P A and Rodwell V W 2000 *Harper's Biochemistry*, 25th edition (Stanford, CT: Appleton & Lange)

Muruganandham M, Kasiviswanathan A, Jagannathan N R, Raghunathan P, Jain P C and Jain V 1999 Diltiazem enhances tumor blood flow: MRI study in a murine tumor; *Int. J. Radiat. Oncol. Biol. Phys.* **43** 413–421

Negendank W 1992 studies of human tumors by MRS: a review; *NMR Biomed.* **5** 303–324

Newman R J, Bore P J, Chan L, Gadian D G, Styles P, Taylor D and Radda G K 1982 Nuclear magnetic resonance studies of forearm muscle in Duchenne dystrophy; *Br. Med. J.* **284** 1072–1074

Ng T C, Comair Y G, Xue N, So N, Majors A, Lolem H, Luders H and Modic M 1994 Temporal lobe epilepsy: presurgical localization with proton chemical shift imaging; *Radiology* **193** 465–472

Noris D G 2001 Implications of bulk motion for diffusion-weighted imaging experiments: effects, mechanisms, and solutions; *J. Magn. Reson. Imaging* **13** 486–495

Ogawa S, Lu T M, Kay A R and Tank D W 1990 Brain magnetic resonance imaging with contrast dependent on blood oxygenation; *Proc. Natl. Acad. Sci. USA* **87** 9868–9872

Ozscunar Y and Sorensen A G 2000 Diffusion- and perfusion-weighted MRI in human acute ischemic stroke: technical considerations; *Top. Magn. Reson. Imaging* **11** 259–272

Pan J W, Hamm J R, Rothman D L and Shulman R G 1988 Intracellular pH in human skeletal muscle by ^{1}H NMR; *Proc. Natl. Acad. Sci. USA* **85** 7836–7839

Petroff O A, Rothman D L, Behar K L, Lamoureux D and Mattson R H 1996 The effect of gabapentin on brain GABA in patients with epilepsy; *Ann. Neurol.* **39** 589–594

Qui H M S, Hedlund L W, Gewalt S L, Benveniste H, Bare T M and Johnson G A 1997 Progression of a focal ischemic lesion in rat brain during treatment with a novel glycine/NMDA antagonist: An *in vivo* 3D diffusion weighted MR microscopy study; *J. Magn. Reason. Imaging* **7** 739–744

Raghunathan P 1999 Magnetic resonance imaging and spectroscopy in biomedicine; *Proc. Indian. Natl. Sci. Acad.* **A65** 87–117

_____ and Jagannathan N R 1996 Magnetic resonance imaging: basic concepts and applications; *Curr. Sci.* **70** 695–708

Rand S D, Prost R and Li S J 1999 Proton spectroscopy of the brain; *Neuroimaging Clin. N. Am.* **9** 379–395

Renshaw P F, Guimaraes A R, Fava M, Rosenbaus J F, Pearlman J D, Flood J G, Puopolo P R, Clancy K and Gonzalez R G 1992 Accumulation of fluoxetine and norfluoxetine in human brain during therapeutic administration; *Am. J. Psychiatry* **149** 1592–1594

Roman B B, Foley J M, Meyer R A and Koretsky A P 1996 Contractile and metabolic effects of increased creatine kinase activity in mouse skeletal muscle; *Am. J. Pathol.* **270** C1236–1245

Rothman D L, Behar K L, Prichard J and Petroff O A 1997 Homocarnoine and the measurement of neuronal pH in patients with epilepsy; *Magn. Reson. Med.* **38** 924–929

_____, Petroff O A, Behar K L and Mattson R H 1993 Localized ^{1}H NMR measurement of GABA in human brain *in vivo*; *Proc. Natl. Acad. Sci. USA* **90** 5662–5666

Rudkin T M and Arnold D L 1999 Proton magnetic resonance spectroscopy for diagnosis and management of cerebral disorders; *Arch. Neurol.* **56** 919–926

Salerno M, Altes T A, Mugler J P 3rd Nakatsu M, Hatubu H and De Lange E E 2001 Hyperpolarized noble gas MR imaging of the lung: potential clinical applications; *Eur.J Radiol.* **40** 33–44

Sandstede J J, Pabst T, Beer M, Lipke C, Baurle K, Butter F, Harre K, Kenn W, Voelker W, Neupauser S and Hahn D 2001 Assessment of myocardial infarction in humans with Na-23 MR imaging; comparison with cine MR imaging and delayed contrast enhancement; *Radiology* **221** 222–228

Sauer D, Allegrini P R and Fagg G E 1994 The competitive N M D A antagonist CGP 40116 is a potent neuroprotectant in a rat model of focal cerebral ischemia; *J. Neural. Trans. Suppl.* **43** 81–89

Sauter A and Rudin M 1990 Calcium antagonists for reduction of brain damage in stroke; *J. Cardiovasc. Pharmac.* **15** (Suppl. 1) 543–547

Sauter P, Rudin M and Wiederhold K H 1988 Reduction of neural damage in irreversible cerebral ischemia by calcium antagonists; *Neurochem. Pathol.* **9** 211–236

Scriver C R, Beaudet A L, Syl W S and Valle D (eds.) 1989 *Metabolic Basics of Inherited Disease*, 6th edition (New York: McGraw Hill)

Segebarth C M, Baleriaux D F, de Beer R, van Ormondt D, Marien A, Luyten P R and den Hollander J A 1989 ^{1}H image guided localized ^{31}P MR spectroscopy of human brain: quantitative analysis of ^{31}P MR spectroscopy measured on volunteers and on intracranial tumor patients; *Magn. Reson. Med.* **11** 349–366

Shapiro E M, Borthakur A, Gougoutas A and Reddy R 2002 ^{23}Na MRI accurately measures fixed charge density in articular cartilage; *Magn. Reson. Med.* **47** 284–291

Shaw T M and Elsken R H 1950 Nuclear magnetic resonance absorption in hygroscopic materials; *J. Chem. Phys.* **18** 1113–1114

Shukla Dave A, Gupta R K, Roy R, Husain N, Paul L, Venkatesh S K, Rashid M R, Chhabra D K and Husain M 2001 Prospective evaluation of *in vivo* proton MR spectroscopy in differentiation of similar appearing intra cranial cystic lesions; *Magn. Reson. Imaging* **19** 103–110

Sijens P J, Huang Y, Baldwin N J and Ng T C 1999 ^{19}F magnetic resonance spectroscopy studies of the metabolism of 5-fluorouracil in murine RIF-1 tumors and liver; *Cancer Res.* **51** 1384–1390

Singer J R 1959 Blood flow rates by nuclear magnetic resonance measurements; *Science* **130** 1652–1653

Sinha K, Degaonkar M N, Jagannathan N R and Gupta Y K 2001 Effect of melatonin on ischemic reperfusion injury induced by middle cerebral artery occlusion in rats; *Eur. J. Pharmacol.* **428** 185–192

Stark D D and Bradley W G 1998 *Magnetic Resonance Imaging* (New York: Mosby).

Stevens A N, Morris P G, Iles R A, Sheldon P W and Griffiths J R 1984 5-Fluorouracil metabolism monitored by *in vivo* ^{19}F NMR; *Br. J. Cancer* **50** 113–17

Swanson M G, Vigneron D B, Tran T K C and Kurhanewicz J 2001 Magnetic resonance imaging and spectroscopic imaging of prostate cancer; *Cancer Invest.* **19** 510–523

Thompson J E, Castillo M and Kwock L 1998 Magnetic resonance spectroscopy in the evaluation of epilepsy; in *Clinical Applications of Magnetic Resonance Spectroscopy* pp33–48 ed. S K Mukherji (New York: Willey-Liss)

Tomoi M, Kimura H, Yoshida M, Itoh S, Kawamura Y, Hayashi N, Yamamoto K, Kubota J and Ishi Y 1997 Alterations of lactate (+ lipid) concentration in brain tumors with *in vivo* hydrogen magnetic resonance spectroscopy during radiotherapy; *Invest. Radiol.* **32** 288–296

Van der Wall E E and de Ross A 1991 *Magnetic Resonance Imaging in Coronary Artery Disease* (Kluwer Academic Publishers)

Van Sluis R, Bhujwalla Z M, Raghunand N, Ballesteros P, Alvarez J, Cerdan S, Galons J P and Gillies R J 1999 *In vivo* imaging of extracellular pH using ^{1}H MRSI; *Magn. Reson. Med.* **41** 743–750

Vanda V J, Sherman J H and Luciano D S 1990 *Human Physiology* (London: McGraw Hill)

Venkatesh S K, Gupta R K, Pal L, Husain N and Husain M 2001 Spectroscopic increase in choline signal is a nonspecific marker for differentiation of infective/inflammatory from neoplastic lesions of the brain; *J Magn. Reson. Imaging* **14** 8–15

von Schulthess G K 1997 Echo-planar imaging; in: *Magnetic Resonance Imaging of the Body* (3rd edn); pp 87–100 eds H Higgins and A Helms (Philadelphia: Lippincot-Raven)

Wielopolski P A, Geuns R J M, de Feyter and Qudkerk M 1998 VCATS: Breathhold coronary MR angiography with volume targeted imaging; *Radiology* **209** 209–219

Wolf W, Presant C A, Servis K L, El-Tahtawy A, Albright M J, Barker P B, Ring III R, Atkinson D, Ong R, King M, Singh M, Ray M, Wiseman C, Blayney D and Shani J 1990 Tumor trapping of 5-fluorouracil: *in vivo* ^{19}F NMR spectroscopic pharmacokinetics in tumor bearing humans and rabbits; *Proc. Natl. Acad. Sci. USA.* **87** 492–496

_____, Albright M J, Silver M S, Weber H, Reichardt V and Sauer R. 1987 Fluorine-19 NMR spectroscopic studies of the metabolism of 5-flurouracil in the liver of patients undergoing chemotherapy; *Magn. Reson. Imaging* **5** 165–169

Wood P J and Hirst D G 1989 Calcium antagonists as radiation modifiers: site specificity in relation to tumor response; *Int. J. Radiat. Oncol. Biol. Phys.* **16** 1141–1144

_____ and _____ 1989 Modification of tumor response by calcium antagonist in the SCVII/St tumor implanted at two different sites; *Int. J. Radiat. Biol.* **56** 355–367

Younkin D P, Berman P, Sladky J, Chee G, Bank W and Chance B 1987 ^{31}P NMR studies in Duchenne muscular dystrophy: age related metabolic changes; *Neurology* **37** 165–169